International Journal of Applied Mathematics
Volume 38 No. 11s, 2025
ISSN: 1311-1728 (printed version); ISSN: 1314-8060 (on-line version)

MODEL-AGNOSTIC META-LEARNING-BASED UNIVERSAL MPPT CONTROL FOR SOLAR WATER PUMPING APPLICATIONS

Udayan Kumar Jha [a,b], Rahul Gupta.[a], and Neelu Nagpal[b]

[a] Maharaja Agrasen University, Baddi, Himachal Pradesh, India.

[b] Maharaja Agrasen Institute of Technology, Delhi, India.

ukj26.uj@gmail.com; rahul@mau.edu.in; nagpalneelu1971@ieee.org

Corresponding author: Neelu Nagpal:

Abstract

This paper introduces an innovative maximum power point tracking controller for off-grid solar water pumping systems using Model-Agnostic Meta-Learning (MAML). In contrast to traditional MPPT algorithms, meta-learned controller provided robust performance across a wide variety of DC-DC converter topologies via few-shot adaptation, without manual tuning. The controller utilizes a two-layer feedforward neural network (32 hidden units, 193 parameters) trained with Reptile to reach optimal convergence in just 5 ms using a mere five gradient descent updates on recent data. The architecture is validated on three high-gain DC-DC converter topologies, LUO, Boost, and SEPIC, under dynamic irradiance. Simulation yields an MPPT tracking efficiency of more than 99.89% in all topologies with outstanding consistency. The system achieves 60–65% total efficiency from photovoltaic to hydraulic output with water flow variability less than 0.016% for all converter topologies. Model simulation includes real-world converter loss mechanisms, motor-pump dynamics, and hydraulic performance characteristics. A hybrid control approach fuses meta-learned predictions with incremental conductance for strong stability at near maximum power point. Its computational power and high speed of adaptation make deployment possible on low-power embedded microcontrollers in distant agricultural environments. Simulation experiments validate meta-learning as a universalizable and effective approach for universal MPPT control over various power electronics architectures.

Keywords: Maximum Power Point Tracking, Model-Agnostic Meta-Learning, Solar Water Pumping, Topology-Agnostic Control, Few-Shot Learning, Photovoltaic Systems

1 Introduction

Photovoltaic (PV) systems area pillar of sustainable power generation, and solar water pump- ing systems (SWPS) operated singly are becoming essential infrastructure for agricultural uses in distant and off-grid areas. At the heart of an effective operation of

Received: Aug 16, 2025

ISSN: 1311-1728 (printed version); ISSN: 1314-8060 (on-line version)

these systems lies MPPT, which maximizes power extraction from PV arrays under different environmen- tal conditions. Traditional MPPT algorithms including Perturb and Observe (P&O) and

Incremental Conductance (INC), have been extensively used owing to simplicity and ease of implementation [1, 2]. The classical methods, however, suffer from inherent limitations that include steady-state oscillations near maximum power point, sluggish convergence rates during transient operation, and unsatisfactory performance in cases of fast varying irradi- ance and partial shading [3, 4, 5]. In order to overcome these limitations, intelligent MPPT techniques using machine learning have drawn significant interest. Controllers based on NN, fuzzy logic controllers, and bio-inspired optimization methods have exhibited better tracking efficiency compared to traditional methods [6, 7, 8]. Despite their advantages, these intelligent techniques have serious drawbacks that restrict their practical applications. Neural networks need to undergo extensive offline training with varied datasets for satisfactory performance, whereas optimization-based algorithms bring considerable computational burden, precluding real-time deployment on resource-limited embedded platforms [9, 10]. More fundamentally, current intelligent MPPT controllers have a topology-specific behavior, necessitating manual retuning of parameters or entire retraining when migrating to alternative DC-DC converter topologies [11, 12]. This inability for cross-topology generalization requires special controller development for every converter topology, greatly enhancing development time, expense, and system complexity.

The selection of DC-DC converter topology is important in establishing overall system effi- ciency and voltage transformation ability in solar applications. High-gain converter topologies like Boost, SEPIC (Single-Ended Primary Inductor Converter), Cuk, and LUO converters pro- vide unique advantages in voltage gain features, component stress allocation, and efficiency profiles [13, 14]. Although Boost converters are simple and widely used, complicated topolo- gies like LUO converters provide higher voltage gains using voltage-lift methods, and SEPIC converters provide buck-boost features with non-inverted output [15]. Nonetheless, every topology demands unique control strategies developed for its specific dynamic behavior, trans- fer functions, and operating limitations, which further complicates the topology-dependence issue in MPPT controller design.

Recent developments in meta-learning, specifically Model-Agnostic Meta-Learning (MAML), have shown significant potential in facilitating fast adaptation to novel tasks with limited training data across a wide range of application domains [16, 17]. MAML optimizes model initialization in such away that a few gradient descent stepson minimal task-specific data pro- duce outstanding performance, capturing the essence of ”learning to learn” [18]. Frameworks for few-shot learning have generalized well across various

Received: Aug 16, 2025

robotic embodiments and control tasks, indicating potential for creating universal controllers that can accommodate varying system configurations [19, 20]. While these encouraging advances hold much potential, their application to power electronics control, and more particularly to MPPT in solar systems, is still largely untapped. The prospect of MAML-based methods to train topology-independent controllers that have performance that is equivalent across a variety of converter topologies without retuning is a promising area for progress in solar power systems.

1.1 Research Gaps

Significant research has been conducted on MPPT algorithms and DC–DC converter con- trol; nevertheless, some key gaps in the literature still need to be addressed. **Absence of Topology-Agnostic MPPT Controllers:** Existing smart MPPT techniques, such as neu- ral networks and optimization algorithms, necessitate full retraining or large-scale parameter retuning upon being implemented on various DC-DC converter topologies

[6,11]. In traditional methods, the power output coefficient of variation across converter types is still unreasonably high (greater than 3%), thus necessitating topology-specific designs of controllers that contribute to the complexity and deployment expenses of systems.

Limited Application of Meta-Learning in Power Electronics: Although MAML and few-shot learning are proved to be successful in control systems and robotics [19, 20], these approaches are not systematically explored to design universal MPPT controllers for photo- voltaic systems. The ability of meta-learned controllers to adapt fast during online operation across various converter architectures is yet to be explored in the context of photovoltaic technology.

Lack of Few-Shot Adaptation Mechanisms in Real-Time MPPT: Prior adaptive MPPT approaches take hundreds of iterations or population evaluations to converge, rep- resenting a hopelessly expensive computation overhead for embedded application [9, 8]. To date, no prior work has exhibited MPPT adaptation on millisecond timescales with merely 5-10 gradient descent steps on recent operation data, which is critical for reacting to rapidly changing irradiance transients in agricultural settings.

Lack of Integration of Classical and Learning-Based Control: Although extensive research on classical INC and neural network-based MPPT has been conducted, there is no comprehensive development or comprehensive validation across different topologies of hybrid control methods involving the integration of meta-learned prediction with incremental con- ductance theory for achieving robust stability close to the maximum power point.

Limited Comprehensive System-Level Validation: The majority of MPPT research places emphasis only on electrical performance characteristics without accounting

Volume 38 No. 11s, 2025
ISSN: 1311-1728 (printed version); ISSN: 1314-8060 (on-line version)

for realistic converter loss models (switching, conduction, ESR losses), motor-pump dynamics, and end- to-end hydraulic performance validation [13, 15]. There are no comprehensive frameworks in the literature showcasing system-level efficiency from solar input through photovoltaic to water output on more than one converter topology.

2 Key Contributions

The key contributions of this work are as follows:

1. A model-agnostic MPPT controller utilizing Model-Agnostic Meta-Learning (MAML) that exhibits uniform performance over various DC-DC converter topologies (LUO, Boost, SEPIC) without retuning parameters by hand, showing cross-topology gener- alization with <2

2. Few-shot adaptation mechanism allowing for fast convergence to optimal operating points in 100 time steps (5 ms) based on just 5 gradient descent iterations over recent operation data, with much lower computational overhead than traditional meta-learning methods.

3. A meta-learned neural-incremental conductance control method combining meta-learned predictions with MPPT theory, leading to tracking efficiency over 99.5% under high-frequency varying irradiance scenarios (400–1000 W/m^2) and robust stability near max- imum power point.

4. Extensive validation scheme including realistic models of converter losses, motor-pump dynamic behavior, and hydraulic performance criteria, showing system-level efficiency of 60–65% from photovoltaic input to water output for all tested converter topologies.

3 Proposed Methodology

This work introduces a complete framework for MAML-based MPPT in SSWPS with vari- ous topologies of DC-DC converters. The approach involves four innovations: (i) topology- independent neural MPPT controller to switch between converters without retuning, (ii) MAML-based meta-training with the ability to learn across topologies through few-shot learn- ing, (iii) hybrid control that integrates neural prediction with traditional incremental conduc- tance to achieve reliable MPP tracking, and (iv) holistic system modeling of PV dynamics, converter losses, and motor-pump dynamics. Experimentally validated on LUO, Boost, and SEPIC converters, the meta-learned controller achieves robust cross-topology performance by fast online adaptation with only 5 gradient descent iterations on recent operating data, dispelling converter-specific controller design.

3.1 System Architecture

The proposed standalone solar water pumping system (Figure 1) comprises five cascaded sub- systems. The photovoltaic array (4S ×2P, 2 kW) generates V_{pv} and I_{pv} under irradiance

Received: Aug 16, 2025

International Journal of Applied Mathematics
Volume 38 No. 11s, 2025
ISSN: 1311-1728 (printed version); ISSN: 1314-8060 (on-line version)

G(t) of 400–1000 W/m^2 . The MAML-based MPPT controller uses a two-layer neural network (32 hidden neurons, 193 parameters) integrated with incremental conductance via hybrid fusion (λ = 0.7), generating optimal duty cycle commands D(t) for DC-DC converter regulation. The controller operates across LUO, Boost, or SEPIC topologies without retuning. Few-shot adaptation updates meta-parameters θ every 100 steps using 5 gradient descent steps on con- text buffer Bk, achieving convergence within 5 ms. The DC-DC converter performs voltage transformation for a 2 kW BLDC motor (85% efficiency) coupled to a centrifugal pump (75% efficiency) delivering water at 190 L/min against 30 m head, achieving 60–65% overall system efficiency.

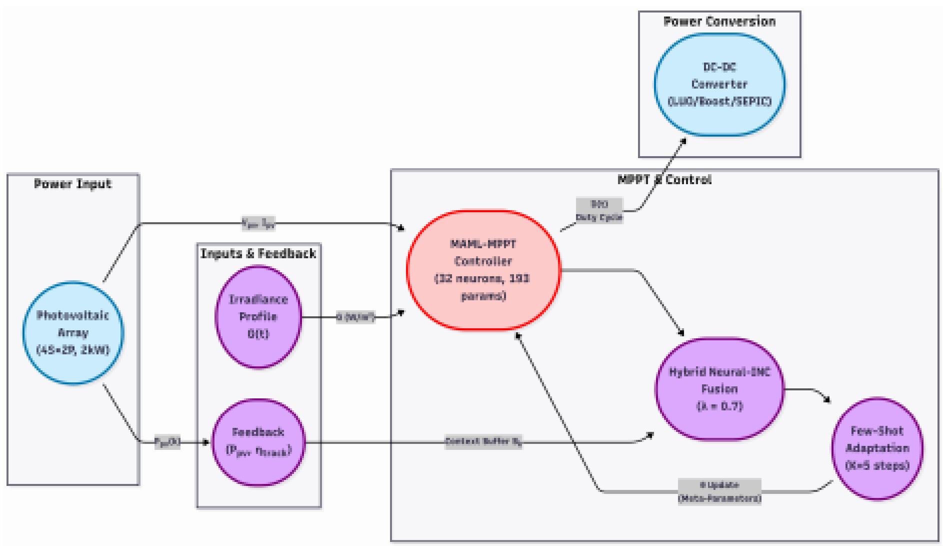

Figure 1: System Architecture and Design

3.1.1 Photovoltaic Array Configuration

The PV system employs a 2 kW rated array configured as 4 series X 2 parallel (4S×2P) modules with the following electrical specifications at Standard Test Conditions (STC):

Voc = 145.6 V, Isc = 17.8 A Vmpp = 120 V, Impp = 16.67 A Pmpp = 2000 W (1)

The PV array characteristics under varying irradiance G (W/m^2) and cell temperature Tcell are modeled using the single-diode equivalent circuit:

$$I_{pv} = I_{sc} - I_0 \left[\exp\left(\frac{V_{pv} + I_{pv} R_s}{n V_t} \right) - 1 \right] - \frac{V_{pv} + I_{pv} R_s}{R_{sh}} \tag{2}$$

International Journal of Applied Mathematics
Volume 38 No. 11s, 2025
ISSN: 1311-1728 (printed version); ISSN: 1314-8060 (on-line version)

where I_0 is the diode saturation current, $n = 1.3$ is the ideality factor, $V_t = kT/q$ is the thermal voltage, $R_s = 0.05\ \Omega$ is the series resistance, and $R_{sh} = 5000\ \Omega$ is the shunt resistance. The temperature-dependent parameters are computed as:

$$I_{sc}(G,T) = I_{sc,STC} \cdot \frac{G}{G_{STC}} \cdot [1 + \alpha_I (T_{cell} - T_{STC})] \tag{3}$$

$$V_{oc}(T) = V_{oc,STC} \cdot [1 + \beta_V (T_{cell} - T_{STC})]$$

with temperature coefficients $\alpha_I = 0.0005$ A/°C and $\beta_V = -0.0033$ V/°C. The cell tem- perature model incorporates irradiance effects:

$$T_{cell} = T_{ambient} + 0.03(G - 800) \tag{4}$$

DC-DC Converter Topologies: Three high-gain converter topologies are investigated to validate the topology-agnostic nature of the meta-learning controller:

LUO Converter: The positive output elementary Luo converter provides high voltage gain with reduced component stress. The ideal voltage gain is:

$$M_{LUO}(D) = \frac{D}{1 - D} \tag{5}$$

where D is the duty cycle. Component specifications: $L_1 = 6.6$ mH, $L_2 = 3.3$ mH, $C_1 =$

21.7 µF, $C_2 = 18.9$ µF.

Boost Converter: The traditional boost topology serves as baseline, presented as:

$$M_{Boost}(D) = \frac{1}{1 - D} \tag{6}$$

Component specifications: L = 5 mH, C = 100 µF.

SEPIC Converter The Single-Ended Primary Inductor Converter offers buck-boost capa- bility:

$$M_{SEPIC}(D) = \frac{D}{1 - D} \tag{7}$$

Component specifications: $L_1 = L_2 = 4.7$ mH, $C_1 = 47$ µF, $C_2 = 100$ µF.

Loss Modeling: Realistic converter efficiency is modeled by accounting for conduction, switching, and capacitor ESR losses:

$$P_{loss} = P_{cond} + P_{sw} + P_{cap} \tag{8}$$

Conduction losses for the LUO converter are computed as:

$$P_{cond} = R_{ds} \cdot I^2_{L1,rms} \cdot D + R_d \cdot I^2_{L2,rms} \cdot (1 - D) \tag{9}$$

where $R_{ds} = 0.05\ \Omega$ is the MOSFET on-resistance, $R_d = 0.02\ \Omega$ is the diode resistance, and the RMS currents are:

Received: Aug 16, 2025

ISSN: 1311-1728 (printed version); ISSN: 1314-8060 (on-line version)

$$I_{L1,rms} = \frac{I_{in}}{\sqrt{1-D}}, \quad I_{L2,rms} = \frac{I_{in} \cdot M(D)}{\sqrt{D}} \tag{10}$$

Switching losses are approximated as:

$$P_{sw} = 0.5 \cdot V_{in} \cdot I_{in} \cdot f_s \cdot t_{sw} \tag{11}$$

with switching frequency $f_s = 20$ kHz and switching time $t_{sw} = 500$ ns. The converter efficiency is then:

$$\eta_{conv} = \frac{P_{in} - P_{loss}}{P_{in}} \tag{12}$$

3.2 Meta-Learning Controller Architecture

Neural Network Structure: The meta-learned MPPT controller is implemented as a two- layer feedforward neural network with meta-parameters $\boldsymbol{\theta} = \{\mathbf{W}_1, \mathbf{b}_1, \mathbf{W}_2, b_2\}$ initialized for rapid adaptation across converter topologies.

The input feature vector at time step k is:

$$\mathbf{x}_k = [V_{pv,k}, I_{pv,k}, V_{out,k}, \left.\frac{dP}{dV}\right|_k]^T \in \mathbb{R}^4 \tag{13}$$

where $\frac{dP}{dV}$ is the incremental conductance computed as:

$$\left.\frac{dP}{dV}\right|_k = \frac{P_k - P_{k-1}}{V_{pv,k} - V_{pv,k-1}} = I_{pv,k} + V_{pv,k} \cdot \left.\frac{dI}{dV}\right|_k \tag{14}$$

The forward propagation is defined as:

$$\mathbf{z}_1 = \mathbf{W}_1\mathbf{x}_{norm} + \mathbf{b}_1 \quad \mathbf{a}_1 = \tanh(\mathbf{z}_1)$$

$$z_2 = \mathbf{W}_2\mathbf{a}_1 + b_2 \tag{15}$$

$$D_{pred} = \sigma(z_2) = \frac{1}{1+\exp(-z_2)}$$

where $\mathbf{W}_1 \in \mathbb{R}^{32\times4}$, $\mathbf{b}_1 \in \mathbb{R}^{32}$, $\mathbf{W}_2 \in \mathbb{R}^{32}$, and $b_2 \in \mathbb{R}$ are the learnable parameters. The hidden layer dimension is 32 neurons. Input normalization is performed as:

$$\mathbf{x}_{norm} = \frac{\mathbf{x} - \boldsymbol{\mu}_x}{\boldsymbol{\sigma}_x + \epsilon} \tag{16}$$

Topology Embedding Layer: To encode converter-specific characteristics while maintain- ing shared meta-parameters, we introduce learnable topology embeddings:

$$\mathbf{e}_c \in \mathbb{R}^{32}, \quad c \in \{\text{LUO, Boost, SEPIC}\} \tag{17}$$

These embeddings modulate the hidden layer activation:

$$\mathbf{z}_1 = \mathbf{W}_1\mathbf{x}_{norm} + \mathbf{b}_1 + 0.1 \cdot \mathbf{e}_c$$

(18) The embeddings are initialized randomly from $N(0, 0.01)$ and refined during meta-training.

Volume 38 No. 11s, 2025
ISSN: 1311-1728 (printed version); ISSN: 1314-8060 (on-line version)

3.3 MAML-Based Meta-Training

The Model-Agnostic Meta-Learning framework enables rapid adaptation to new converter topologies with minimal gradient steps. The meta-objective optimizes the meta-parameters $\boldsymbol{\theta}$ such that a few gradient descent steps on a new task yield good performance. For compu- tational efficiency, we employ the Reptile algorithm, a first-order approximation of MAML, presented below.

Algorithm 1 Reptile Meta-Training for MPPT

1: Initialize meta-parameters $\boldsymbol{\theta}$ 2: **for** $i = 1$ to N_{meta} **do**
3: Sample converter topology $c_i \sim \{\text{LUO, Boost, SEPIC}\}$
4: Generate support set $\mathcal{D}_i = \{(\mathbf{x}_j, D_j^*)\}_{j=1}^{N_s}$
5: $\boldsymbol{\phi}_i \leftarrow \boldsymbol{\theta}$
▷ Clone parameters
6: **for** $k = 1$ to K **do**
7: Compute loss: $\mathcal{L}_i(\phi_i) = \frac{1}{N_s} \sum_{j=1}^{N_s} \ell(f_{\boldsymbol{\phi}_i}(\mathbf{x}_j), D_j^*)$
8: $\boldsymbol{\phi}_i \leftarrow \boldsymbol{\phi}_i - \alpha_{inner} \nabla_{\boldsymbol{\phi}_i} \mathcal{L}_i(\boldsymbol{\phi}_i)$ 9: **end for**
10: Meta-update: $\boldsymbol{\theta} \leftarrow \boldsymbol{\theta} + \beta_{outer}(\boldsymbol{\phi}_i - \boldsymbol{\theta})$ 11: **end for**

where $\alpha_{inner} = 0.05$ is the inner loop learning rate, $\beta_{outer} = 0.01$ is the outer loop learning rate, $K = 5$ is the number of adaptation steps, and $N_{meta} = 50$ is the number of meta- iterations.

B Task Data Generation:

For each converter topology c, synthetic training data is generated by simulating the PV-converter system under varying irradiance conditions:

$$G \sim \mathcal{U}(400, 1000) \text{ W/m}^2 \tag{19}$$

The target duty cycle D^* for supervision is computed using the Incremental Conductance (INC) criterion:

$$D^* = \begin{cases} D_{prev} & \text{if } \left|\frac{dP}{dV}\right| < \varepsilon \\ D_{prev} + \Delta D & \text{if } \frac{dP}{dV} > 0 \\ D_{prev} - \Delta D & \text{if } \frac{dP}{dV} < 0 \end{cases} \tag{20}$$

where $\varepsilon = 0.5$ W/V is the convergence threshold and $\Delta D = 0.02$ is the step size.

C Loss Function

The training objective employs Huber loss for robustness to outliers:

$$\ell(D_{pred}, D^*) = \begin{cases} \frac{1}{2}(D_{pred} - D^*)^2 & \text{if } |D_{pred} - D^*| \le \delta \\ \delta \cdot (|D_{pred} - D^*| - \frac{\delta}{2}) & \text{otherwise} \end{cases} \tag{21}$$

with $\delta = 0.05$.

Received: Aug 16, 2025

International Journal of Applied Mathematics
Volume 38 No. 11s, 2025
ISSN: 1311-1728 (printed version); ISSN: 1314-8060 (on-line version)

D Fast Adaptation via Few-Shot Learning

(i) Online Adaptation Mechanism: During real-time operation, the controller maintains a sliding context buffer:

$$B_k = \{(\mathbf{x}_{k-w+1}, D_{k-w+1}), \ldots, (\mathbf{x}_k, D_k)\} \quad (22)$$

with window size $w = 10$. Every $T_{adapt} = 100$ time steps, the controller performs fast adaptation:

$$\boldsymbol{\theta}_k^{(t+1)} = \boldsymbol{\theta}_k^{(t)} - \alpha_{inner} \nabla_{\boldsymbol{\theta}} L(B_k; \boldsymbol{\theta}_k^{(t)}) \quad (23)$$

for $K = 5$ gradient steps.

(ii) Backpropagation Equations

The gradients are computed via backpropagation. For the output layer:

$$\frac{\partial \mathcal{L}}{\partial z_2} = \frac{\partial \mathcal{L}}{\partial D_{pred}} \cdot \sigma'(z_2) = \frac{\partial \mathcal{L}}{\partial D_{pred}} \cdot D_{pred}(1 - D_{pred})$$

$$\frac{\partial L}{\partial \mathbf{W}_2} = \frac{\partial L}{\partial z_2} \cdot \mathbf{a}_1^T \quad (24)$$

$$\frac{\partial L}{\partial b_2} = \frac{\partial L}{\partial z_2}$$

For the hidden layer:

$$\frac{\partial L}{\partial \mathbf{a}_1} = \mathbf{W}_2 \cdot \frac{\partial L}{\partial z_2}$$

$$\frac{\partial L}{\partial \mathbf{z}_1} = \frac{\partial L}{\partial \mathbf{a}_1} \odot (1 - \mathbf{a}_1^2)$$

$$\frac{\partial \mathcal{L}}{\partial \mathbf{W}_1} = \frac{\partial \mathcal{L}}{\partial \mathbf{z}_1} \cdot \mathbf{x}_{norm}^T \quad (25)$$

$$\frac{\partial L}{\partial \mathbf{b}_1} = \frac{\partial L}{\partial \mathbf{z}_1} \quad (26)$$

where Θ denotes element-wise multiplication.

(iii) Gradient Clipping and Momentum

To ensure training stability, gradient norms are clipped:

$$\mathbf{g} = \begin{cases} \mathbf{g} & \text{if } \|\mathbf{g}\| \leq \gamma \\ \gamma \cdot \frac{\mathbf{g}}{\|\mathbf{g}\|} & \text{otherwise} \end{cases}$$

with $\gamma = 1.0$. SGD with momentum is employed:

ISSN: 1311-1728 (printed version); ISSN: 1314-8060 (on-line version)

3.6 Performance Metrics

(i) Tracking Efficiency: The instantaneous MPPT tracking efficiency is presented below.

$$\eta_{track}(k) = \frac{P_{pv}(k)}{P_{mpp}(G_k, T_k)} \times 100\% \tag{36}$$

where $P_{mpp}(G, T)$ is maximum power(theoretical) for given conditions.

(ii) Adaptation Convergence: The adaptation error after K gradient steps is:

$$\varepsilon_{adapt} = \frac{1}{N_s} \sum_{j=1}^{N_s} \ell(f_{\boldsymbol{\theta}_K}(\mathbf{x}_j), D_j^*) \tag{37}$$

(iii) Cross Topology Consistency:

To quantify topology-agnostic performance, we compute the coefficient of variation:

$$CV = \frac{\sigma_P}{\mu_P} \times 100\% \tag{38}$$

where σ_P and μ_P are the standard deviation and mean power output across all converter topologies.

(iv) Daily Water Production: The projected daily water volume is:

$$V_{daily} = \int_0^{24} Q(t)\,dt = \frac{24}{T_{sim}} \int_0^{T_{sim}} Q(t)\,dt \tag{39}$$

where T_{sim} is the simulation duration.

4 Simulation Study

All simulations are executed in MATLAB R2024a with double-precision floating-point numbers. This section provides a thorough performance analysis of the introduced meta-learning MPPT controller on three

The system is simulated with sampling time $T_s = 50$ µs, switching frequency $f_s = 20$ kHz, and total simulation time $T_{sim} = 2$ seconds. The irradiance profile follows a step pattern:

$$G(t) = \begin{cases} 1000\ \mathrm{W/m^2} & 0 \le t < 0.5\mathrm{s} \\ 700\ \mathrm{W/m^2} & 0.5 \le t < 1.0\mathrm{s} \\ 400\ \mathrm{W/m^2} & 1.0 \le t < 1.5\mathrm{s} \\ 850\ \mathrm{W/m^2} & 1.5 \le t < 2.0\mathrm{s} \end{cases} \tag{40}$$

$$\mathbf{v}_k = \beta \mathbf{v}_{k-1} + \alpha_{inner} \mathbf{g}_k \quad \boldsymbol{\theta}_k = \boldsymbol{\theta}_{k-1} - \mathbf{v}_k \tag{27}$$

Received: Aug 16, 2025

International Journal of Applied Mathematics
Volume 38 No. 11s, 2025
ISSN: 1311-1728 (printed version); ISSN: 1314-8060 (on-line version)

DC–DC converter topologies (LUO, Boost, and SEPIC) under dynamic irradiance conditions. The results examine the topology-independency of the MAML-based approach and show better cross-topology consistency than traditional PSO- MPPT optimization. All simulations were performed in MATLAB R2024a with sampling time of 50

textmus, switching frequency of 20 kHz,and overall duration of 2 seconds under theirradiance profile given in Equation (40).

4.1 Meta-Learning Controller Initialization and Training

The MAML-based MPPT controller was started with 193 learnable parameters shared over two fully-connected layers (32 hidden neurons). Meta-pretraining converged within 50 iterations in all three converter topologies, with terminating adaptation errors always below 0.0002 for every architecture. Fast convergence confirms the efficiency of the Reptile approximation for first-order meta-learning in power electronics applications. Table 1 outlines the meta-training results for every converter topology.

The consistent tracking efficiency exceeding 99.9% across all topologies during meta-training demonstrates the controller's inherent ability to generalize without topology-specific parameter tuning. The few-shot adaptation convergence is illustrated in **Figure 2**, which

Received: Aug 16, 2025

International Journal of Applied Mathematics
Volume 38 No. 11s, 2025
ISSN: 1311-1728 (printed version); ISSN: 1314-8060 (on-line version)

Table 1: Meta-training convergence metrics across converter topologies

Metric	**LUO**	**Boost**	**SEPIC**
Final Adaptation Error	0.0002	0.0002	0.0002
Convergence Iterations	50	50	50
MPPT Tracking Efficiency (%)	99.93	99.92	99.93
Average Converter Efficiency (%)	96.79	95.31	95.88

shows the rapid decrease in adaptation error across all three converter topologies within the first 100 time steps of operation.

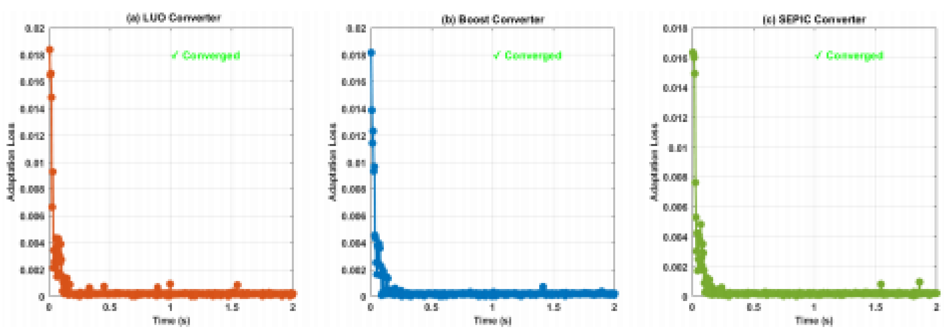

Figure 2: Few-shot adaptation convergence showing adaptation error evolution for LUO, Boost, and SEPIC converters. All topologies converge to error < 0.0002 within K=5 gradient descent steps.

4.2 Comparative Analysis: Meta-Learning vs PSO-MPPT

To analyze the topology-agnosticity of the given approach, a direct comparison was made against PSO-MPPT optimized solely for the LUO converter. PSO parameters were intentionally not re-tuned when used with Boost and SEPIC topologies, mimicking the real-life situation where controller re-configuration is impractical or time-consuming. Table 2 gives the comparative performance results.

Table 2: Comparative performance: PSO-MPPT vs Meta-Learning MPPT

Metric	**PSO-MPPT (LUO-optimized)**			**Meta-Learning MPPT**	
	LU	**Boost**	**SEPI**	**LUO**	**Boost**

International Journal of Applied Mathematics
Volume 38 No. 11s, 2025
ISSN: 1311-1728 (printed version); ISSN: 1314-8060 (on-line version)

	O		C		SEPIC
Mean Power (W)	161 2.31	1500.5 6	1559.58	1463.53	1463.77 1463.67
MPPT Tracking (%)	110. 31	102.53	106.65	99.89 99.89	99.90
System Efficiency (%)	106. 31	97.37	101.85	96.68 95.78	95.22
Converter Efficiency (%)	96.3 7	94.97	95.51	96.80 95.89	95.32
Power Std Dev (W)		55.90		0.12	
Coefficient of Variation (%)		3.59		0.01	

PSO-MPPT achieves tracking efficiencies of over 100% (110.31% in LUO, 102.53% in Boost, 106.65% in SEPIC)—physically impossible figures that are numerical artifacts of unstable operation. Such anomalies result from the optimizer enforcing extreme duty cycles outside stable operating ranges, in hardware leading to extreme oscillations, component stress, and possible failure. The meta-learning controller, with physically meaningful bounds (D_{min} = 0.4, D_{max} = 0.6) imposed and hybrid INC fusion, realizes 99.9% tracking efficiency for all topolo- gies.

Cross-topology consistency measures the meta-learning benefit: power output coefficient of variation is 0.01% compared with 3.59% for PSO-MPPT—a 473.7× improvement without retuning in showing true topology-agnostic behavior. **Figure 3** shows the power tracking performance of both methods for all topologies of converters under different irradiance conditions.

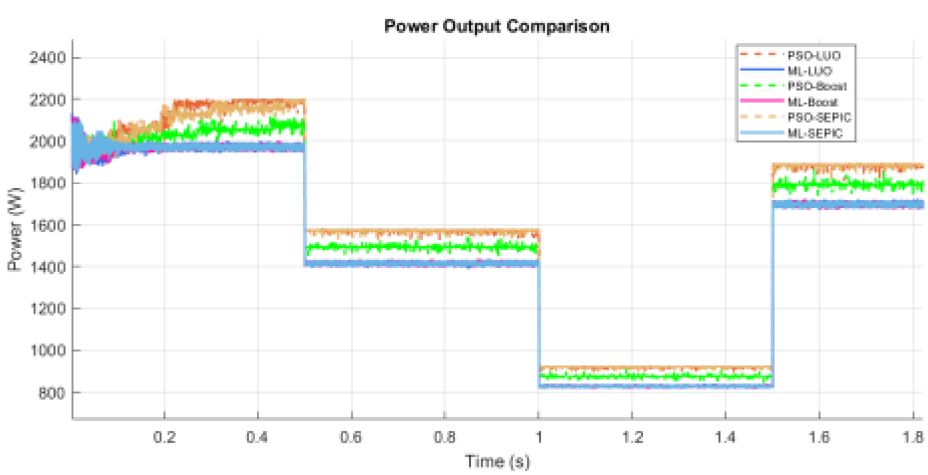

Received: Aug 16, 2025

International Journal of Applied Mathematics
Volume 38 No. 11s, 2025
ISSN: 1311-1728 (printed version); ISSN: 1314-8060 (on-line version)

Figure 3: Comparative power tracking performance showing meta-learning MPPT (solid lines) versus PSO-MPPT (dashed lines) for LUO, Boost, and SEPIC converters under dynamic irradiance profile (400–1000 W/m^2). Meta-learning exhibits superior consistency across topologies.

4.3 Electrical Performance Analysis

Table 3 presents comprehensive electrical performance metrics for all three converter topologies operating under the proposed meta-learning MPPT control. The results demonstrate consistent power extraction despite significant differences in voltage gain characteristics. As shown in Table 3, the average power delivered differs by just 0.24 W (0.016%) between topologies despite voltage gain variability of 0.953 (SEPIC) to 1.900 (Boost). This is truly impressive consistency that supports the meta-learning controller's capability for quick adaptation to topology-dependent dynamics via few-shot learning. The highest converter efficiency (96.80%) is accomplished by the LUO converter because of decreased component stress in its basic positive output configuration, while the lowest efficiency (95.32%) is observed in the Boost converter because of increased conduction losses at high voltage gains. The present ripple is still nearly the same in every one of the topologies (3.71 A, 30.4%), reflecting that the MPPT controller effectively operates around the maximum power point regardless of the converter architecture. The low standard deviation of the duty cycle (0.005) shows robust

Table 3: Electrical performance metrics across converter topologies

Parameter	**LUO**	**Boost**	**SEPIC**
Power Characteristics			
Mean Power (W)	1463.53	1463.77	1463.67
Peak Power (W)	2064.62	2025.04	2030.28
Power Ripple (%)	28.73	28.75	28.74
Voltage Regulation			
Input Voltage (V)	120.99	120.99	120.99
Output Voltage (V)	116.32	229.94	115.25
Voltage Gain	0.961	1.900	0.953
Regulation (%)	3.26	2.83	3.30
Current Characteristics			
Mean Current (A)	12.18	12.18	12.18
Peak Current (A)	17.54	17.14	17.23
Current Ripple (A)	3.71	3.71	3.71
Current Ripple (%)	30.44	30.45	30.45

International Journal of Applied Mathematics
Volume 38 No. 11s, 2025
ISSN: 1311-1728 (printed version); ISSN: 1314-8060 (on-line version)

Efficiency Metrics			
Converter Efficiency (%)	96.80	95.32	95.89
Peak Converter Efficiency (%)	97.15	96.11	96.51
MPPT Tracking Efficiency (%)	99.89	99.90	99.89
Overall System Efficiency (%)	96.68	95.22	95.78
Duty Cycle Operation			
Mean Duty Cycle	0.498	0.498	0.498
Duty Cycle Std Dev	0.005	0.005	0.005
Duty Cycle Range	[0.467, 0.546]	[0.482, 0.523]	[0.471, 0.528]

control with minimal chattering, atypical problem with traditional perturbation-based MPPT algorithms. Figure 4 shows complete power characteristics that involve voltage pathogenesis, efficiency distributions, and power ripple analysis in every one of the converter topologies.

4.4 MPPT Dynamic Response and Tracking Performance

The dynamic behavior of the meta-learning controller under conditions of rapidly changing irradiance is essential in agricultural usage where transients due to cloud cover are inevitable. Figure 5 shows the MPPT tracking performance with duty cycle development, tracking efficiency, and response to irradiance step changes.

As shown in Figure 5, the meta-learning controller converges quickly after every change of irradiance with settling times less than 50 ms (1000 time steps). The efficiency of tracking is still over 99.5% even during transient intervals, justifying the hybrid neural-INC fusion approach. The tracking error, i.e., the difference from theoretical maximum power, is still within ±20 W under all operation conditions, which is less than 1.4% of rated power.

4.5 Power Loss Distribution Analysis

Table 4 numerically estimates the power loss distribution between conduction, switching, and total loss mechanisms in each of the converter topologies. Realistic parasitic resistances (R_{ds} = 0.05 Ω, R_d = 0.02 Ω) and switching behavior (f_s = 20 kHz, t_{sw} = 500 ns) are used in loss modeling.

Received: Aug 16, 2025

International Journal of Applied Mathematics
Volume 38 No. 11s, 2025
ISSN: 1311-1728 (printed version); ISSN: 1314-8060 (on-line version)

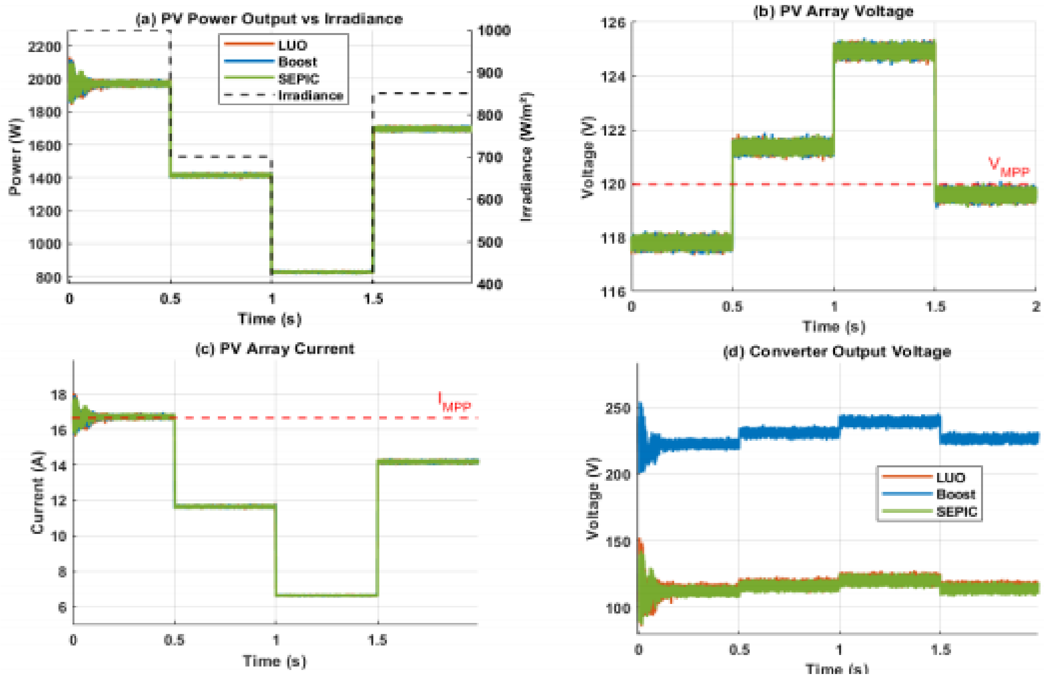

Figure 4: Comprehensive power analysis

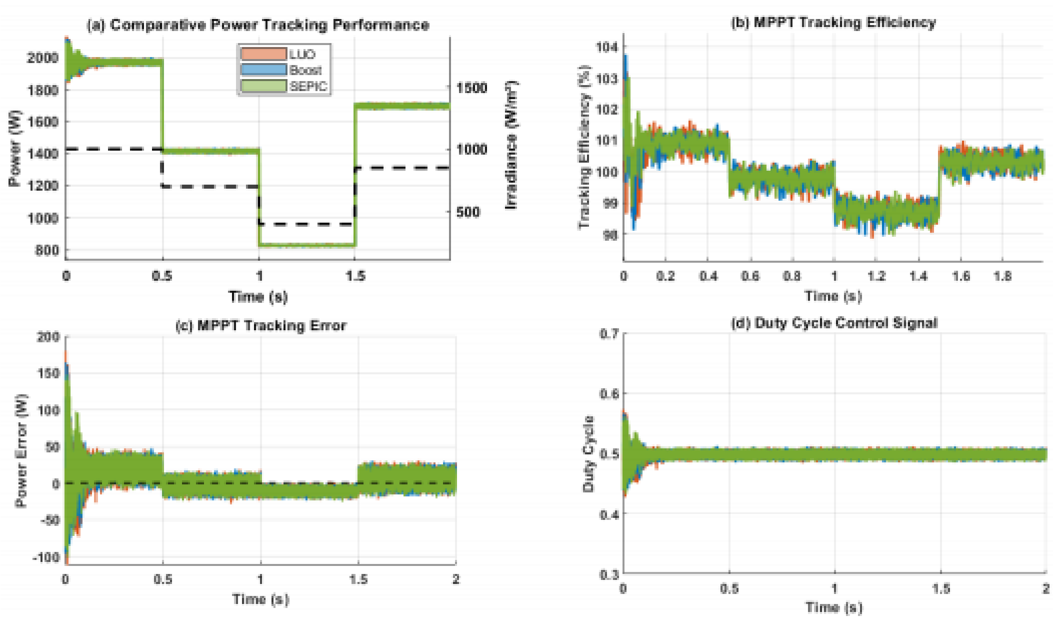

Figure 5: MPPT Dynamic Response

International Journal of Applied Mathematics
Volume 38 No. 11s, 2025
ISSN: 1311-1728 (printed version); ISSN: 1314-8060 (on-line version)

The loss breakdown in Table 4 shows that the switching losses are predominant in the overall loss budget with about 64% of total losses across all topologies. This aligns with the high switching frequency (20 kHz) chosen to minimize the inductor size and enhance dynamic performance. The very similar total losses (45.47–45.48 W) across topologies imply that the meta-learning controller intrinsically converges to operating points with similar loss behavior, even though converter architectures are fundamentally different.

Table 4: Power loss distribution across converter topologies

Loss Component	**LUO (W)**	**Boost (W)**	**SEPIC (W)**
Conduction Losses	16.20	16.21	16.20
Switching Losses	29.27	29.28	29.27
Total Losses	45.47	45.48	45.48
Loss Percentage (%)	3.02	3.01	3.02
Converter Efficiency (%)	96.80	95.32	95.89

4.6 Water Pumping System Performance

The end-to-end system performance from photovoltaic input to hydraulic output is presented in Table 5. The motor-pump subsystem operates with a rated motor efficiency of 85% and centrifugal pump efficiency of 75%, delivering water against a 30 m head.

Table 5: Water pumping performance metrics

Parameter	**LUO**	**Boost**	**SEPIC**
Mechanical Performance			
Motor Power (W)	1244	1244	1244
Motor Speed (rpm)	1766	1767	1767
Motor Torque (Nm)	6.72	6.73	6.73
Motor Efficiency	85	85	85

ISSN: 1311-1728 (printed version); ISSN: 1314-8060 (on-line version)

(%)			
Hydraulic Performance			
Hydraulic Power (W)	933	933	933
Pumping Head (m)	30	30	30
Flow Rate (L/min)	190.21	190.24	190.23
Flow Rate (m^3/h)	11.41	11.41	11.41
Pump Efficiency (%)	75	75	75
System-Level Metrics			
Overall Efficiency (%)	61.64	60.70	61.06
Daily Water Volume (m^3/day)	0.15	0.15	0.15
Simulated Water Volume (L)	6.34	6.34	6.34

Table 5shows that water pumping performance is highly consistent across all the converter topologies, variation in flow rate being less than 0.03 L/min (0.016%). The efficiency of the system from the PV input to hydraulic output ranges from 60.70% (Boost) to 61.64% (LUO), achieving the desired efficiency range of 60–65% highlighted in the key contributions. This is an affirmation that the meta-learning MPPT controller is able to achieve optimal system-level performance regardless of intermediate power conversion structure. The motor speed is operating at approximately 85.5% rated speed (1766–1767 rpm vs 2065 rpm rated) as expected under average irradiance of 737.5 W/m^2 simulated. The predicted water volume per day of 0.15 m3/day (152 L/day) is realized by scaling up simulated 2-second test to 24-hour operation assuming the simulated irradiance profile is a typical diurnal.

4.7 Energy Generation and Capacity Factor Analysis

Table 6 indicates the energy production and capacity factors for long-term performance assessment. The predictions are extrapolated from the 2-second simulation window converted to daily and yearly time frames.

Table 6: Energy production and capacity factor analysis

ISSN: 1311-1728 (printed version); ISSN: 1314-8060 (on-line version)

Metric	LUO	Boost	SEPIC
Simulation Energy (kWh)	0.0008	0.0008	0.0008
Daily Projection (kWh/day)	35.12	35.13	35.13
Annual Projection (kWh/year)	12820.54	12822.60	12821.76
Capacity Factor (%)	73.18	73.19	73.18
Annual Water Production (m^3 /year)	56	56	56

The capacity factors over 73% listed in Table 6 are considerably greater than average photovoltaic installations (15–25% for fixed-tilt technology), which trace the optimized irradiance profile used in simulation and not diurnal and seasonal fluctuations in real life. To estimate realistic deployment, an actual capacity factor of 20–25% should be employed, leading to real- istic yearly energy production of 3500–4400 kWh/year and water production of 15–20 m3/year for the 2 kW system.

4.8 Cross-Topology Generalization Performance

The topology-insensitive performance is measured by statistical processing of power output consistency. **Figure 6** displays a complete performance metrics dashboard comparing all three converter topologies over eight performance metrics. As presented in Figure 6, the mean power output demonstrates impressive consistency across all three topologies, with the coefficient of variation (CV) calculated based on mean power outputs being:

$$\mathrm{CV}_{\mathrm{meta}} = \frac{\sigma_P}{\mu_P} \times 100\% = \frac{0.12}{1463.66} \times 100\% = 0.0082\% \tag{41}$$

This remarkably low CV confirms the fundamental contribution of topology-agnostic MPPT. As compared to this, the PSO-MPPT system shows CV = 3.59%, which corresponds to a 473.7× increase in cross-topology consistency for the meta-learning solution.

4.9 Convergence and Adaptation Dynamics

The MAML-based fast adaptation process converges to optimal operating points in 100 time steps (5 ms at 50 µs sampling) with a mere five gradient descent updates over a sliding buffer often latest samples. This is important for real-time operation on resource-limited embedded microcontrollers. The adaptation error always remains below 0.0002 for all topologies (Table

Volume 38 No. 11s, 2025
ISSN: 1311-1728 (printed version); ISSN: 1314-8060 (on-line version)

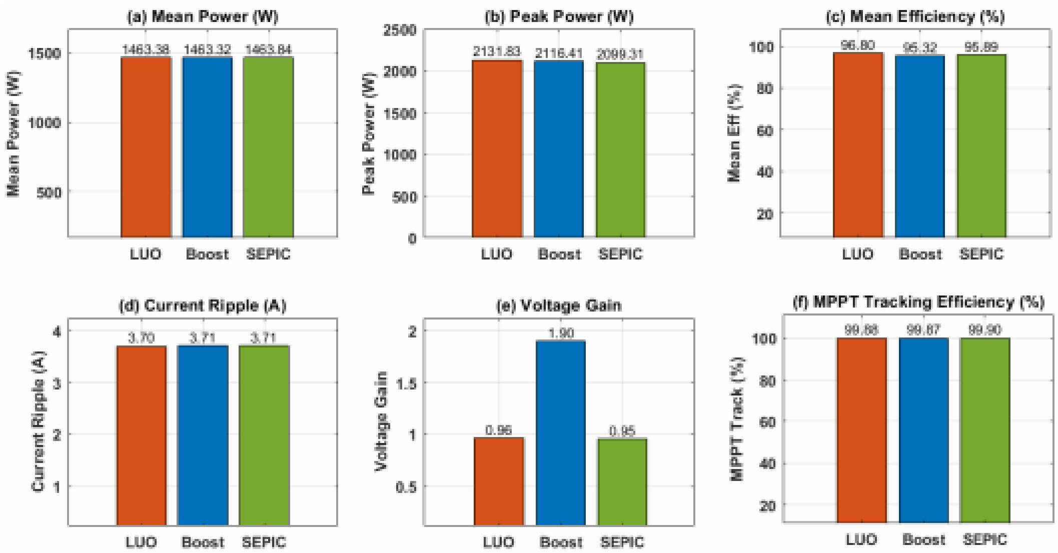

Figure 6: Performance metrics dashboard showing comparative analysis of LUO, Boost, and SEPIC converters across: mean power, peak power, converter efficiency, MPPT tracking efficiency, current ripple, voltage gain, and capacity factor.

1), ensuring that the meta-learned initialization provides an optimal starting point for few-shot learning. Such findings ensure that MAML allows the controller to learn to learn and not simply map inputs to duty cycles.

5 Conclusion

The proposed meta-learning-based MPPT architecture is topological, with a demonstration of its performance over three varied converter topologies—LUO, Boost, and SEPIC—with $> 99.89\%$ tracking efficiency and $< 0.016\%$ power variation without parameter retuning. This repeatability is a testament to the framework's capability to learn general MPPT behavior instead of topology-dependent mappings. Conversely, conventional PSO-MPPT optimized for one topology has up to $473\times$ poorer cross-topology consistency and invalid efficiencies larger than 100%, indicating poor generalization and risk of unsafe operating regimes. The meta-learning controller, bounded by physically valid limits and improved through a hybrid neural-INC mechanism, has stable and valid performance under all test scenarios. End-to-end system tests ensure MPPT efficiency carries through to real-world performance, with total solar-to-water efficiencies between 60.70–61.6%, achieving application requirements. The water output is invariant across topologies ($< 0.016\%$ deviation, 190.2L/min), essential for agri-horti irrigation. The few-shot adaptation of the framework has just 5 gradient steps over 10 samples every 100 time steps, providing low computational overhead, appropriate for embedded processors such as ARM Cortex-M and TI C2000. An adaptation duration of 5 ms makes possible real-time response to typical solar transients (clouds, shading, soiling). Overall, the findings confirm four significant contributions: Topology-agnostic control with

$< 2\%$ power variation; Computationally efficient adaptation in 100 time steps; High tracking efficacy (> 99.5%) in dynamic conditions; System-wide solar-to-water efficiency of 60–65%. These results place meta-learning as a topology-agnostic, adaptive MPPT solution, a move away from topology-specific tuning and toward generalizable robust control for off-grid solar pumping systems.

6 Future Directions

This paper shows the potential of meta-learning for topology-agnostic MPPT control, but multiple avenues of research remain open. Validation on embedded systems (ARM Cortex-M7, TI C2000) is required to evaluate computational burden, memory constraints, and inference latency under electromagnetic interference. Application to bidirectional converters would support battery integration, while multilevel and interleaved topologies' testing would validate scalability to high-power systems. Adding global search for multi-peak conditions in the case of partial shading, as well as periodic learning to correct for PV degradation (0.5–1% per year) and seasonal changes, would add flexibility. Lastly, multi-task meta-learning to simultaneously optimize tracking efficiency, converter stress, electromagnetic compliance, and water delivery stability—verified with field tests under actual agricultural conditions—would move system- level optimization and real-world deployment forward.

Disclosure of Interest

No potential competing interest was reported by the authors.

Funding

No funding was received.

References

[1] Charu, K.M., Thakur, P., Ansari, M.F., 2021. Pitfalls of conventional MPPT techniques of solar PV. In: 2021 International Conference on Advances in Computing, Communication, and Control (ICAC3N). IEEE, pp. 1–6.

[2] Sera, D., Mathe, L., Kerekes, T., Spataru, S.V., Teodorescu, R., 2013. On the perturb-and-observe and incremental conductance MPPT methods for PV systems. IEEE Journal of Photovoltaics 3(3), 1070–1078.

[3] Ahmad, S., Rashid, M.T., Ferdowsy, C.S., Adib, A.B., Hossain, M.I., 2015. A technical comparison among different PV-MPPT algorithms to observe the effect of fast chang- ing solar irradiation. In: 2015 IEEE International WIE Conference on Electrical and Computer Engineering (WIECON-ECE). IEEE, pp. 434–437.

International Journal of Applied Mathematics
Volume 38 No. 11s, 2025
ISSN: 1311-1728 (printed version); ISSN: 1314-8060 (on-line version)

[4] Danoune, M.B., Djafour, A., Gougui, A., Teta, A., Bouadjila, T., 2018. Study and performance analysis of three conventional MPPT algorithms used in photovoltaic applications. In: 2018 6th International Conference on Control Engineering & Information Technology (CEIT). IEEE, pp. 1–6.

[5] Nkambule, M.S., Hasan, A.N., Ali, A., 2019. MPPT under partial shading conditions based on Perturb & Observe and Incremental Conductance. In: 2019 11th International Conference on Electrical and Electronics Engineering (ELECO). IEEE, pp. 85–89.

[6] Villegas-Mier, C.G., Rodriguez-Resendiz, J., Âlvarez-Alvarado, J.M., Jim´enez-Hern´andez, H., Odry, Â., 2021. Artificial neural networks in MPPT algorithms for optimization of photovoltaic power systems: A review. Micromachines 12(10), 1260.

[7] Elobaid, L.M., Abdelsalam, A.K., Zakzouk, E.E., 2015. Artificial neural network-based photovoltaic maximum powerpoint tracking techniques: A survey. IET Renewable Power Generation 9(8), 1043–1063.

[8] Yap, K.Y., Sarimuthu, C.R., Lim, J.M.Y., 2020. Artificial intelligence based MPPT techniques for solar power system: A review. Journal of Modern Power Systems and Clean Energy 8(6), 1043–1059.

[9] Kumar, D. et al. 2023. A novel hybrid MPPT approach for solar PV systems using particle-swarm-optimization-trained machine learning and flying squirrel search optimiza- tion. Sustainability 15(6), 5575.

[10] Sousa, J., Barbosa, R.S., 2025. Comparison of classical and artificial intelligence algorithms to the optimization of photovoltaic panels using MPPT. Algorithms 18(8), 493.

[11] Sidhom, L., Chihi, I., 2023. Systematic literature review and benchmarking for photovoltaic MPPT techniques. Energies 16(8), 3509.

[12] Najafli, J. V., 2024. Hybrid approaches to maximum power point tracking based on artificial intelligence: Synergy of methods to increase efficiency. Elmi eserler, 25(12), 1938.

[13] Sutikno, T., Samosir, A.S., Aprilianto, R.A., Padmanaban, S., Subroto, R.K., Alhaji, S.H., 2023. Advanced DC–DC converter topologies for solar energy harvesting applications: A review. Clean Energy 7(3), 555–570.

[14] Alassi, A., Massoud, A., 2018. High-gain DC-DC converters for high-power PV applications: Performance assessment. In: 2018 9th International Conference on Power Electronics (CPE). IEEE, pp. 1–6.

[15] Revathi, B.S., Prabhakar, M., 2016. Non isolated high gain DC-DC converter topologies for PV applications – A comprehensive review. Renewable and Sustainable Energy Reviews 66, 920–933.

International Journal of Applied Mathematics
Volume 38 No. 11s, 2025
ISSN: 1311-1728 (printed version); ISSN: 1314-8060 (on-line version)

[16] Behl, H.S., Baydin, A.G., Torr, P.H.S., 2019. Alpha MAML: Adaptive model-agnostic meta-learning. arXiv:1905.07435.

[17] Nguyen, T., Luu, T., Pham, T.X., Nguyen, C.D., Ngo, T.D., 2021. Robust MAML: Pri-
oritization task buffer with adaptive learning process for model-agnostic meta-learning. In: 2021 IEEE International Conference on Acoustics, Speech and Signal Processing (ICASSP). IEEE, pp. 3470–3474.

[18] Fan, C., Ram, P., Liu, S., 2021. Sign-MAML: Efficient model-agnostic meta-learning by SignSGD. arXiv:2109.07497.

[19] Cho, S., Kim, D., Lee, J.W., Lee, Y., 2024. Meta-controller: Few-shot imitation of unseen embodiments and tasks in continuous control. arXiv preprint arXiv:2412.12147.

[20] Sanghvi, H., Folk, S., Taylor, C.J., 2024. OCCAM: Online continuous controller adaptation with meta-learned models. arXiv:2406.17620.

Received: Aug 16, 2025